

## **Spin-polarized transport in magnetic tunnel junctions with ZnTe barriers**

W. G. Wang <sup>1</sup>, C. Ni <sup>2</sup>, A. Ozbay <sup>1</sup>, L. R. Shah <sup>1</sup>, X. Fan <sup>1</sup>,  
X.M. Kou <sup>1</sup>, E.R. Nowak <sup>1</sup>, and J. Q. Xiao <sup>1</sup>

*1) Department of Physics and Astronomy, University of Delaware, Newark, DE 19716, USA*

*2) Department of Materials Science and Engineering, University of Delaware, Newark, DE 19716, USA*

Magnetic tunnel junctions with wide band gap semiconductor ZnTe barrier were fabricated. A very low barrier height and sizable magnetoresistance were observed in the Fe/ZnTe/Fe junctions at room temperature. The nonlinear I-V characteristic curve confirmed the observed magnetoresistance is due to spin-dependent tunneling effect. Temperature dependent study indicated that the total conductance of the junction is dominated by direct tunneling, with only a small portion from the hopping conduction through the defect states inside the barrier.

Magnetic tunneling junctions (MTJs) have wide application in hard disk read head, magnetic random access memory, ultra-low field sensor and many other devices.<sup>1-3</sup> Giant tunneling magnetoresistance (TMR) can be achieved in the MTJs with crystalline MgO barrier.<sup>4,5</sup> In the coherent tunneling process, combination of the symmetry filtering property of MgO and the highly spin-polarized electrons with  $\Delta_1$  symmetry in Fe or CoFe electrodes gives rise to the large TMR effect.<sup>6,7</sup> Here the most important feature of MgO-(001) tunnel barrier is that the  $\Delta_1$  evanescent state has the lowest decay rate, while other evanescent states with  $\Delta_5$ ,  $\Delta_2$  or  $\Delta_2'$  symmetry decay much faster. Compared to traditional  $\text{Al}_2\text{O}_3$  barrier, MgO shows superior performance at small thickness. Therefore MgO barrier is commonly used in the read head of hard disk drives. Though generally speaking for MRAM applications MTJs with perpendicular magnetic anisotropy are preferred,<sup>8-11</sup> for hard disk read heads the focus is still at the resistance-area (RA) product. For example in hard disks with density higher than  $2\text{Tb/in}^2$ , which requires a RA product smaller than  $0.3\Omega\mu\text{m}^2$  simultaneously with a TMR larger than 50%, the use of MgO tunnel barrier may not be desirable.<sup>12,13</sup> This is primarily due to the large forbidden gap of MgO (7.8 eV),<sup>14</sup> which posts intrinsic limitation for reducing the barrier height below 0.35 eV.<sup>5,15</sup> Therefore, it is of great importance to explore new barrier materials that possess similar electronic structure as MgO but with lower barrier heights.

In this work, we report the study on the room temperature tunneling magnetoresistance in MTJs with ZnTe barriers. Similar to MgO, the lowest orbital of the conduction band in the (001) direction of ZnTe has  $\Delta_1$  symmetry. A large TMR was predicated with ZnSe,<sup>16</sup> which shares very similar electronic band structure with ZnTe. Compared common barrier materials such as  $\text{Al}_2\text{O}_3$  and MgO, ZnTe has a much lower band gap of 2.2 eV.<sup>17</sup> Therefore, a large TMR and small RA could potentially be realized in junctions with ZnTe barriers. ZnTe has a stable zinc blende phase with a lattice constant of 0.61nm.<sup>17</sup> It has important applications in Terahertz imaging,<sup>18</sup> tunneling diode,<sup>19</sup> solar-cells contacts<sup>20</sup> and diluted magnetic semiconductors.<sup>21,22</sup> Our study shows that a very low barrier height (0.13 eV) can be obtained in junctions with ZnTe barriers. A tunneling magnetoresistance of 3.5% is observed at RT. The spin-polarized transport

across the Fe/ZnTe interface demonstrated here also paves the way for studying spin manipulation in ZnTe at room temperature.

Samples in this study were fabricated in a vacuum chamber equipped with 6 sputtering sources, one plasma source and one ion source. The base pressure of the system is  $5 \times 10^{-8}$  Torr. The sample structures were Si/Cu 70/ IrMn 15 / CoFe 6/Fe 1.6/ZnTe(1-3)/Fe 1.6/CoFe 12/Cu 50 (numbers indicate layer thickness in nanometers). The Si(001) wafers were treated by HF and properly cleaned before loading into the chamber. The layers below ZnTe barrier were chosen so that the bottom Fe interface is (001) oriented. In the current study, the barrier layers were deposited at RT and 160°C. After the fabrication of blanket films, MTJs with diameters ranging from 5 $\mu$ m to 100 $\mu$ m were defined by standard microfabrication process including multiple steps of photolithography and ion-beam milling. The RT transport measurement was performed in the standard 4-probe configuration on a probe station. The low temperature properties were tested in a PPMS system. More details in the MTJ fabrication and testing techniques are described by our previous publications.<sup>23-25</sup>

The structure of unpatterned MTJ films was first characterized by x-ray diffraction. As shown in Figure 1(a), the film stack below ZnTe barrier is (001)-oriented. The CoFe(001) layer was grown on IrMn(001) despite a large lattice mismatch of 6.3%.<sup>26</sup> The Cu (311) peak at about 90 degree is from the capping layer as it is absent in the sample without top Cu layers ( not shown). The lattice mismatch between Fe(001) and ZnTe(001) is 6.4%. Therefore a Fe(001)/ZnTe(001)/Fe(001) epitaxial sandwich structure could possibly be achieved just as the case of Fe(001)/MgO(001)/Fe(001) junctions, thus lead to high TMR ratios.<sup>6,16</sup> The cross-sectional transmission electron microscopy (TEM) study was carried out to investigate the microstructure of the barrier layer. A uniform ZnTe barrier with very small roughness can be grown on the Fe electrode as shown in Figure 1(b). The distinct interfaces between the ZnTe barrier and the Fe electrodes can be clearly seen. However, the ZnTe barrier exhibits amorphous nature as shown in the high resolution image in Figure 1(c). The barrier layer was also found amorphous when ZnTe was deposited at 160°C. The RF sputtering power and Ar pressure used for the ZnTe barrier was 40 W and 4.5 mTorr, respectively. Further investigation on the effect of

sputtering power, inner gas pressure and substrate temperature is necessary to optimize the barrier structure.

The room temperature TMR ratios for junctions with difference barrier thickness are shown in Figure 2(a). TMR values around 2% were obtained in a wide range of barrier thicknesses when ZnTe was deposited at RT. On the other hand, TMR quick decreases with reducing barrier thickness when ZnTe was deposited at 160°C. The optimal barrier thickness for the highest TMR is 2.3nm and 2.6nm, respectively, for barriers deposited at RT and 160°C. The dependence of the antiparallel RA of the MTJs on the barrier thickness is shown in Figure 2(b). Due to the much lower band gap of ZnTe, the RAs in ZnTe MTJs are generally more than 3 orders of magnitude lower than the RAs in MgO junctions with the same barrier width. The tunneling resistance in junctions with RT-deposited barrier scales almost linearly with barrier thickness in the log scale. In the WKB approximation, the slope of resistance versus barrier thickness curve can be expressed as  $4\pi(2m\phi)^{1/2}/h$ ,<sup>27</sup> where  $m$  is the electron mass,  $\phi$  is the barrier height and  $h$  is the Planck's constant. From the slope we can estimate the barrier height of ZnTe is about 0.13 eV. This value is substantially lower than MgO (0.35-0.4 eV)<sup>5,15</sup> and much lower than ZnS (~0.58 eV).<sup>28</sup> The TMR ratios can be improved by post-growth thermal annealing. The highest TMR in the present study is 3.5% after the MTJs were annealed at 200°C as shown in Figure 2(c). The TMR curve show a very sharp switch at around 25 Oe, indicating very flat barrier-electrode interfaces as observed in the TEM pictures. The tunneling characteristics is confirmed by the nonlinear IV curve of the junction as shown in the inset of Figure 2(c), which demonstrates the observed magnetoresistance is due to tunneling instead of GMR effect.

It is important to characterize the percentage of spin independent contribution to the total conductance due to thermal excitation in our junctions with semiconducting barriers. The temperature dependence of TMR is shown in Figure 3(a). The TMR almost linearly increases with decreasing temperature. In general, the total conductance in a MTJ can be expressed by the model proposed by Shang *et al* as,<sup>29</sup>

$$G(\theta) = G_T (1 + P_1 P_2 \cos \theta) + G_{SI} \quad \text{Eq. (1)}$$

, where the first term is from the direct spin-dependent tunneling; the second term,  $G_{SI}$ , is from spin-independent conduction. The direct tunneling conductance coefficient  $G_T$  only depends weakly on temperature and can be treated as constant.<sup>29</sup> Then for our junction with Fe as both top and bottom electrodes the TMR can be described by the extended Julliere's formula,

$$TMR = 2P^2 / (1 - P^2 + G_{SI} / G_T) . \quad \text{Eq. (2)}$$

By assuming the spin polarization of the ferromagnetic electrode has the same temperature dependence as surface magnetization (thus following the  $T^{3/2}$  rule), the conductance difference between parallel and antiparallel configuration can be expressed as  $\Delta G = 2G_T P^2 = 2G_T P_0^2 (1 - \alpha T^{3/2})^2$ , where  $P_0$  is the zero temperature spin polarization at the Fe/ZnTe interfaces.  $\Delta G$  can be fit with the equation above as shown in Figure 3(b). The best fit value for  $\alpha$  is  $2 \times 10^{-5} \text{ K}^{-3/2}$ , consistent with previous report.<sup>30</sup> Now the spin independent conductance due to thermal excitation can be calculated by  $G_{SI} = \langle G \rangle - G_T$ , where  $\langle G \rangle$  is the average conductance between parallel and antiparallel configuration.  $G_T$  can be derived from the fitting of  $\Delta G$ . The temperature dependence of  $G_{SI}$  is shown in the inset of Figure 3(b). The behavior of  $G_{SI}$  can be explained by the electron hopping through the defect states inside the ZnTe barrier. The hopping process is greatly activated upon increasing temperature.  $G_{SI}$  can be well fit by  $\sigma_0 + \sigma_2 T^{1.33}$ , corresponding to the hopping through 2 localized states in the ZnTe barrier.<sup>31</sup> The defect states assisted hopping conduction was also observed in junctions with  $\text{Al}_2\text{O}_3$ ,<sup>23,29</sup>  $\text{MgO}$ <sup>30</sup> and  $\text{ZnSe}$ <sup>32</sup> barrier. It also has a large impact to the noise level of the MTJs.<sup>33</sup> In the early study on MTJs with ZnSe barrier, it was found spin independent conduction dominates at RT due to the defect states assisted hopping.<sup>34</sup> In our junctions  $G_{SI}$  only accounts for about 10% of total conductance at RT as shown in the inset of Figure 3(b), demonstrating good barrier quality despite the amorphous nature of ZnTe. The TMR in this system now can be readily calculated by using Equation 2. The experimental data can be well represented by the calculation as shown in Figure 3(a).

To summarize, we have investigated the spin-dependent transport properties in MTJs with ZnTe as barriers. ZnTe has been identified as a potential candidate for achieving ultra-low RA values in MTJs. The barrier height of ZnTe estimated by WKB approximation is only 0.13 eV, much lower than most other tunneling barrier. A TMR ratio of 3.5% was observed at RT. Upon further optimization, a substantial enhancement of TMR is possible in junctions with crystalline ZnTe barrier through the coherent tunneling mechanism. The spin-polarized transport across the Fe/ZnTe interface demonstrated here will also help future study on manipulation of spin in ZnTe.

#### ACKNOWLEDGEMENT

This work was supported by DOE DE-FG02-07ER46374 and NSF Grant No. DMR0827249.

#### REFERENCES

- 1 Yuasa, S. & Djayaprawira, D. D. Giant tunnel magnetoresistance in magnetic tunnel junctions with a crystalline MgO(001) barrier. *J. Phys. D-Appl. Phys.* **40**, R337-R354 (2007).
- 2 Gallagher, W. J. & Parkin, S. S. P. Development of the magnetic tunnel junction MRAM at IBM: From first junctions to a 16-Mb MRAM demonstrator chip. *IBM J. Res. & Dev.* **50**, 5-23 (2006).
- 3 Egelhoff Jr., W. F. *et al.* Critical challenges for picoTesla magnetic-tunnel-junction sensors. *Sensors and Actuators A: Physical* **155**, 217-225 (2009).
- 4 Parkin, S. S. P. *et al.* Giant tunnelling magnetoresistance at room temperature with MgO (100) tunnel barriers. *Nature Materials* **3**, 862-867 (2004).
- 5 Yuasa, S., Nagahama, T., Fukushima, A., Suzuki, Y. & Ando, K. Giant room-temperature magnetoresistance in single-crystal Fe/MgO/Fe magnetic tunnel junctions. *Nature Materials* **3**, 868-871 (2004).

- 6 Butler, W. H., Zhang, X.-G., Schulthess, T. C. & MacLaren, J. M. Spin-dependent tunneling conductance of Fe|MgO|Fe sandwiches. *Physical Review B* **63**, 054416 (2001).
- 7 Mathon, J. & Umerski, A. Theory of tunneling magnetoresistance of an epitaxial Fe/MgO/Fe(001) junction. *Physical Review B* **63**, 220403 (2001).
- 8 Apalkov, D., Dieny, B. & Slaughter, J. M. Magnetoresistive Random Access Memory. *Proceedings of the IEEE* **104**, 1796-1830 (2016).
- 9 Almasi, H., Xu, M., Xu, Y., Newhouse-Illige, T. & Wang, W. G. Effect of Mo insertion layers on the magnetoresistance and perpendicular magnetic anisotropy in Ta/CoFeB/MgO junctions. *Applied Physics Letters* **109**, 032401 (2016).
- 10 Almasi, H. *et al.* Perpendicular magnetic tunnel junction with W seed and capping layers. *Journal of Applied Physics* **121**, 153902 (2017).
- 11 Xu, M. *et al.* Voltage-Controlled Antiferromagnetism in Magnetic Tunnel Junctions. *Physical Review Letters* **124**, 187701 (2020).
- 12 Fuke, H. N., Hashimoto, S., Takagishi, M. & Iwasaki, H. MR Enhancement of CPP-SV with FeCo nanocontacts for 2Tb/in<sup>2</sup>. *11th Joint MMM-Intermag Conference, Washington DC CC-02* (2010).
- 13 Katine, J. A. & Fullerton, E. E. Device implications of spin-transfer torques. *Journal of Magnetism and Magnetic Materials* **320**, 1217-1226 (2008).
- 14 Roessler, D. M. & Walker, W. C. Electronic Spectrum and Ultraviolet Optical Properties of Crystalline MgO. *Physical Review* **159**, 733 LP - 738 (1967).
- 15 Hayakawa, J., Ikeda, S., Matsukura, F., Takahashi, H. & Ohno, H. Dependence of giant tunnel magnetoresistance of sputtered CoFeB/MgO/CoFeB magnetic tunnel junctions on MgO barrier thickness and annealing temperature. *Japanese Journal of Applied Physics Part 2-Letters & Express Letters* **44**, L587-L589 (2005).
- 16 MacLaren, J. M., Zhang, X. G., Butler, W. H. & Wand, X. D. Layer KKR approach to Bloch-wave transmission and reflection: Application to spin-dependent tunneling. *Physical Review B* **59**, 5470-5478 (1999).
- 17 Bhargava, R. Properties of Wide Bandgap II-VI Semiconductors. *Properties of Wide Bandgap II-VI Semiconductors* (Inspec. London (1997).).
- 18 Blanchard, F. *et al.* Generation of 1.5  $\mu$ J single-cycle terahertz pulses by optical rectification from a large aperture ZnTe crystal. *Optics Express* **15**, 13212-13220 (2007).

- 19 Agarwal, K. C., Saito, H., Yuasa, S. & Ando, K. Growth and transport studies in M/I/p-SC magnetic tunnel diodes containing different tunnel barrier materials. *Ieee Transactions on Magnetics* **43**, 2809-2811 (2007).
- 20 Gessert, T. A., Li, X., Coutts, T. J., Mason, A. R. & Matson, R. J. Dependence of Material Properties of Radiofrequency Magnetron-Sputtered, Cu-Doped, Znte Thin-Films on Deposition Conditions. *Journal of Vacuum Science & Technology a-Vacuum Surfaces and Films* **12**, 1501-1506 (1994).
- 21 Saito, H., Zayets, V., Yamagata, S. & Ando, K. Room-temperature ferromagnetism in a II-VI diluted magnetic semiconductor Zn<sub>1-x</sub>Cr<sub>x</sub>Te. *Physical Review Letters* **90** (2003).
- 22 Wang, W. G. *et al.* Microstructure, magnetic, and spin-dependent transport properties of (Zn,Cr)Te films fabricated by magnetron sputtering. *Physical Review B (Condensed Matter and Materials Physics)* **77**, 155207-155207 (2008).
- 23 Wang, W. G. *et al.* Spin-polarized transport in hybrid (Zn,Cr)Te/Al<sub>2</sub>O<sub>3</sub>/Co magnetic tunnel junctions. *Applied Physics Letters* **88**, 202501 (2006).
- 24 Wang, W. G. *et al.* Real-time evolution of tunneling magnetoresistance during annealing in CoFeB/MgO/CoFeB magnetic tunnel junctions. *Applied Physics Letters* **92**, 152501 (2008).
- 25 Liu, Y. Z., Wang, W. G., Moriyama, T., Xiao, J. Q. & Zhang, Z. Direct measurement of barrier asymmetry in AlO<sub>x</sub>/ZrO<sub>y</sub> magnetic tunnel junctions using off-axis electron holography. *Physical Review B* **75**, 134420 (2007).
- 26 Moriyama, T., Ni, C., Wang, W. G., Zhang, X. & Xiao, J. Q. Tunneling magnetoresistance in (001)-oriented FeCo/MgO/FeCo magnetic tunneling junctions grown by sputtering deposition. *Applied Physics Letters* **88**, 222503 (2006).
- 27 Simmons, J. G. Electric Tunnel Effect between Dissimilar Electrodes Separated by a Thin Insulating Film. *Journal of Applied Physics* **34**, 2581-& (1963).
- 28 Guth, M., Dinia, A., Schmerber, G. & van den Berg, H. A. M. Tunnel magnetoresistance in magnetic tunnel junctions with a ZnS barrier. *Applied Physics Letters* **78**, 3487-3489 (2001).
- 29 Shang, C. H., Nowak, J., Jansen, R. & Moodera, J. S. Temperature dependence of magnetoresistance and surface magnetization in ferromagnetic tunnel, junctions. *Physical Review B* **58**, R2917-R2920 (1998).
- 30 Kou, X., Schmalhorst, J., Thomas, A. & Reiss, G. Temperature dependence of the resistance of magnetic tunnel junctions with MgO barrier. *Applied Physics Letters* **88**, 212115-212113 (2006).



- 31 Glazman, L. I. & Matveev, K. A. Inelastic Tunneling through Thin Amorphous Films. *Zhurnal Eksperimentalnoi I Teoreticheskoi Fiziki* **94**, 332-343 (1988).
- 32 Jiang, X., Panchula, A. F. & Parkin, S. S. P. Magnetic tunnel junctions with ZnSe barriers. *Applied Physics Letters* **83**, 5244-5246 (2003).
- 33 Stearrett, R., Wang, W. G., Shah, L. R., Xiao, J. Q. & Nowak, E. R. Magnetic noise evolution in CoFeB/MgO/CoFeB tunnel junctions during annealing. *Applied Physics Letters* **97**, 243502 (2010).
- 34 Gustavsson, F., George, J. M., Etgens, V. H. & Eddrief, M. Structural and transport properties of epitaxial Fe/ZnSe/FeCo magnetic tunnel junctions. *Physical Review B* **64**18 (2001).

## FIGURES CAPTIONS

Figure 1(color online). (a).  $\theta$ -2 $\theta$  X-ray diffraction pattern of the MTJ film. (b) Cross-sectional TEM image of the sample. (c) High resolution TEM image of the sample for the barrier region.

Figure 2(color online). (a) Dependence of TMR on the barrier thickness for MTJs, with ZnTe barrier fabricated at RT (square) and 160°C (dot). (b) Dependence of RA on the barrier thickness. The straight lines are the fit by the WKB approximation for determining the barrier height. (c) TMR curve of the MTJ after post-growth annealing at 200°C. Inset shows the I-V curve of the junction.

Figure 3(color online). (a) Temperature dependence of TMR (square) and the fit by the extended Julliere formula (solid line). (b) Temperature dependence of  $\Delta G$  and the fit based on  $T^{3/2}$  rule. Inset shows the ratio of the spin independent conductance to the total conductance and the fit based on the defect states assisted hopping picture.

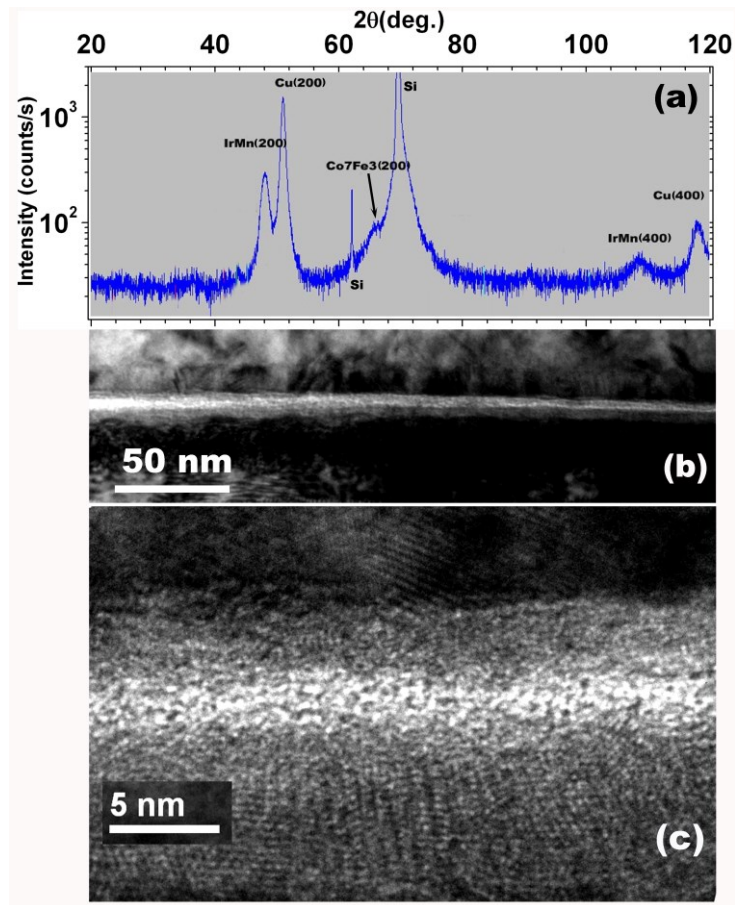


Figure 2(color online). (a).  $\theta$ -2 $\theta$  X-ray diffraction pattern of the MTJ film. (b) Cross-sectional TEM image of the sample. (c) High resolution TEM image of the sample for the barrier region.

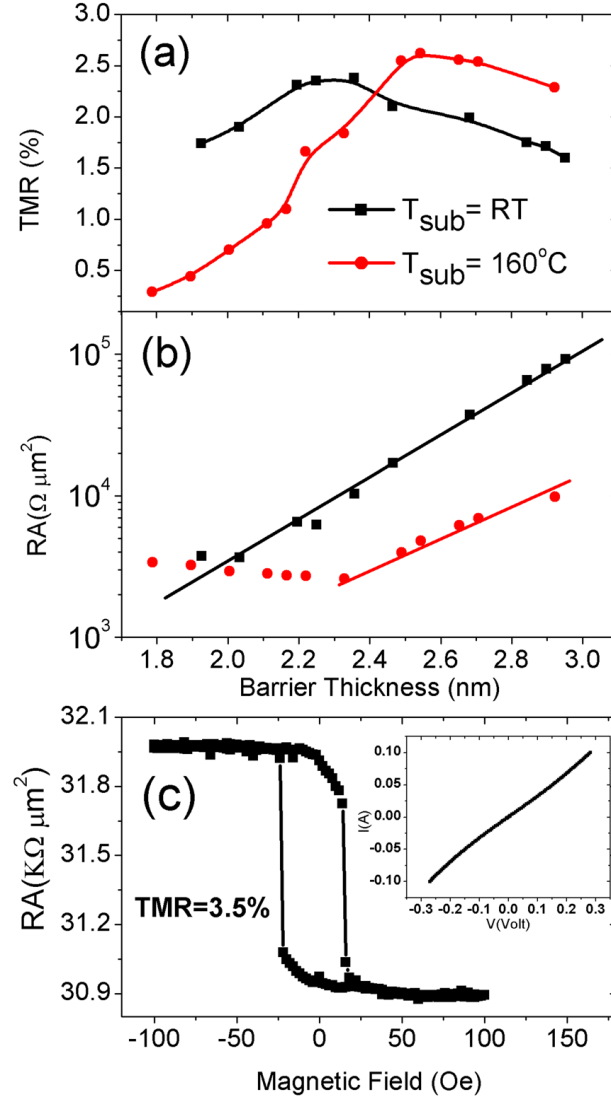


Figure 2(color online). (a) Dependence of TMR on the barrier thickness for MTJs, with ZnTe barrier fabricated at RT (square) and 160°C (dot). (b) Dependence of RA on the barrier thickness. The straight lines are the fit by the WKB approximation for determining the barrier height. (c) TMR curve of the MTJ after post-growth annealing at 200°C. Inset shows the I-V curve of the junction.

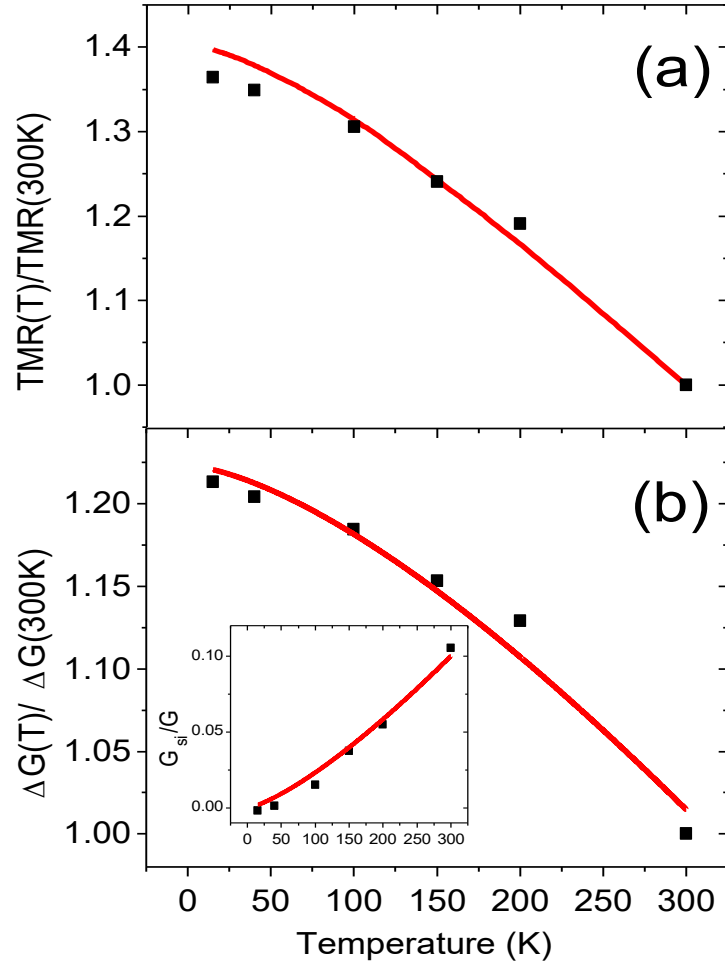


Figure 3 (color online). (a) Temperature dependence of TMR (square) and the fit by the extended Julliere formula (solid line). (b) Temperature dependence of  $\Delta G$  and the fit based on  $T^{3/2}$  rule. Inset shows the ratio of the spin independent conductance to the total conductance and the fit based on the defect states assisted hopping picture.